

Cascade-induced synchrony in stochastically driven neuronal networksKatherine A. Newhall,¹ Gregor Kovačič,¹ Peter R. Kramer,¹ and David Cai^{2,3,*}¹*Mathematical Sciences Department, Rensselaer Polytechnic Institute, 110 8th Street, Troy, New York 12180, USA*²*Department of Mathematics, Shanghai Jiao Tong University, Shanghai 200240, China*³*Courant Institute of Mathematical Sciences and Center for Neural Science, New York University, 251 Mercer Street, New York, New York 10012-1185, USA*

(Received 2 December 2009; revised manuscript received 9 August 2010; published 1 October 2010)

Perfect spike-to-spike synchrony is studied in all-to-all coupled networks of identical excitatory, current-based, integrate-and-fire neurons with delta-impulse coupling currents and Poisson spike-train external drive. This synchrony is induced by repeated cascading “total firing events,” during which all neurons fire at once. In this regime, the network exhibits nearly periodic dynamics, switching between an effectively uncoupled state and a cascade-coupled total firing state. The probability of cascading total firing events occurring in the network is computed through a combinatorial analysis conditioned upon the random time when the first neuron fires and using the probability distribution of the subthreshold membrane potentials for the remaining neurons in the network. The probability distribution of the former is found from a first-passage-time problem described by a Fokker-Planck equation, which is solved analytically via an eigenfunction expansion. The latter is found using a central limit argument via a calculation of the cumulants of a single neuronal voltage. The influence of additional physiological effects that hinder or eliminate cascade-induced synchrony are also investigated. Conditions for the validity of the approximations made in the analytical derivations are discussed and verified via direct numerical simulations.

DOI: [10.1103/PhysRevE.82.041903](https://doi.org/10.1103/PhysRevE.82.041903)

PACS number(s): 87.19.lc, 87.19.lj, 87.19.ln, 05.10.Gg

I. INTRODUCTION

Synchronous neuronal-network oscillations are a ubiquitous phenomenon, occurring in diverse areas of the brain, with great complexity of manifestations, a multitude of frequency ranges, a host of presumed underlying physiological mechanisms reflecting an intricate interplay among short- and long-range, excitatory, and inhibitory interneuronal connections, and often involving large numbers of neurons [1–6]. While the role of synchronous oscillations in various brain functions is not yet well understood, they are believed to serve as clocks and means of information encoding [6,7].

One broad type of neuronal-network oscillations is a collective phenomenon in which only the membrane potentials and spiking averaged over an entire network of neurons exhibit oscillations, whereas the individual neuronal potential and spiking may not appear oscillatory [8–13]. Such oscillations can be detected for example, by measuring the local field potential, i.e., the average neuronal membrane potential in a patch of cortical tissue, which reflects the overall neuronal activity in this patch [14–18].

A different type of neuronal-network oscillations involves primarily excitatory neurons, firing in bursts, such as in developing networks [19–23]. These bursts emerge from a quiescent state and are believed to be suppressed by refractoriness caused by either synaptic depression [22] or an adaptation current [21,23].

Due to the large numbers of neurons involved, network models used in computational studies of various types of synchronous oscillations frequently consist of simplified point neurons of integrate-and-fire type. The model networks

have been either all-to-all coupled [24] or sparse [25–27], composed of excitatory [22,23,28], inhibitory [29–35] or both types of neurons [36–41], homogeneous [42], or heterogeneous [43,44], and driven deterministically [24] or randomly [13], and thus have yielded a great variety of network mechanisms responsible for synchronous behavior and ways to compute the respective oscillation frequencies.

Considering very basic point-neuron and neuronal-network models is important because they often produce the clearest and most sharply delineated network mechanisms responsible for a given type of network dynamics. Among the most basic is the current-based, all-to-all coupled, excitatory, integrate-and-fire (IF) model [45–47]. Under *constant* drive sufficiently strong to push the neuronal voltages over the firing threshold, i.e., *superthreshold* drive, this network is known to synchronize for almost all initial conditions and exhibit time-periodic *total firing events*, during which all the neurons fire at once [24]. This synchrony is induced by the attraction in the phase dynamics of the neurons in the network. Small randomness in the coupling [48] and other model parameters [49] does not destroy this synchrony.

In this paper, we consider a fully stochastic version of this classic model, in which we replace the (nearly) constant external drive by a noisy drive, with each neuron driven by an independent Poisson spike train. We reveal a different mechanism for the perfect spike-to-spike synchrony, namely, *cascading total firing events* which drive the network to synchrony after a period of effectively zero coupling. Under certain parameter regimes, the network exhibits nearly periodic dynamics, switching between effectively totally uncoupled states and cascading states when all neurons fire together. This cascade mechanism of synchrony can operate both in the *superthreshold* regime when the average of the external drive is sufficiently strong to push the neuronal voltages over the firing threshold, and, more importantly, in the

*cai@cims.nyu.edu

subthreshold regime when it is not, and the neuronal firing is driven by fluctuations in the external drive. In both regimes, cascading total firing events are separated by random time intervals, but with a well-defined mean frequency. We should emphasize that these total firing events differ from their deterministic counterparts in that the individual neuronal-voltage trajectories are now not identical but instead differ from neuron to neuron. Therefore, total firing events occur not because of complete synchrony of the voltage trajectories, as in the deterministic case, but rather as cascading events during which the firing of one neuron pushes the next neuron's voltage over threshold, and so on, when the neuronal voltages are not spread too far apart.

After presenting numerical evidence of persistent synchronous cascading total firing events in the network, we derive the average time-period between pairs of neighboring total firing events using a first-passage-time approach [50–55] and solving the associated Fokker-Planck equation via an eigenfunction expansion. What makes this approach possible is the above-mentioned fact that, between cascading total firing events, no neurons fire, and thus the network is effectively decoupled. The approach works for both subthreshold and superthreshold external drives. In addition, we develop a Gaussian approximation to describe the spreading of the neuronal voltages between total firing events, and use it for an alternative derivation of the average oscillation frequency in the regime of superthreshold driving. In this framework, we moreover develop a combinatorial argument to calculate the probability of observing repeated cascading total firing events.

Finally, we discuss how additional physiological effects affect the synchrony of firing events. These include synaptic failure, sparsity of synaptic connections, random transmission delays, and finite rise and decay times for the neuronal conductances. We see that the first two effects act in a similar fashion. They preserve cascading total firing events, but reduce the probability of observing these events in succession, proportionally to the average reduction of network connectivity. The last two effects destroy cascading total firing events and turn them into approximate synchrony, provided the transmission delays or conductance time scales are not too long. In particular, we give numerical evidence that all neurons still fire within short, approximately periodic time-intervals, interspersed with longer quiescent periods.

The remainder of the paper is organized as follows. We discuss the current-based integrate-and-fire model in Sec. II along with a brief description of the event-driven algorithm used for numerical simulation. In Sec. III, we begin our discussion of the synchronous dynamics present in this model. We proceed with analysis of the completely synchronous state in Sec. IV by deriving the mean time between total firing events, and an approximation to this time, based on the Gaussian approximation of a single neuronal-voltage distribution derived in Sec. IV B 1. These results are compared to the results from numerical simulation in Sec. IV C. To complete the discussion of the synchronous dynamics, in Sec. V we compute the probability of finding repeated total firing events, and obtain excellent agreement with the corresponding numerical simulation results. Using this measure of synchrony, we investigate how effective additional physiological

effects are at reducing synchronous behavior in Sec. V C. Conclusions are presented in Sec. VI. Further details of the analysis are presented in the Appendix.

II. MODEL

We consider a model neuronal network of N all-to-all coupled, current-based, excitatory, integrate-and-fire (IF), point neurons [45,46], governed by the system of equations

$$\frac{dv_j}{dt} = -g_L(v_j - V_R) + I_j(t), \quad j = 1, \dots, N, \quad (1a)$$

where v_j is the membrane potential of the j th neuron, g_L is the leakage conductance, and V_R is the leakage/reset voltage. The voltage, v_j , evolves according to Eq. (1a) while it remains below the firing threshold, V_T . The synaptic current, $I_j(t)$, is modeled by the pulse train

$$I_j(t) = f \sum_l \delta(t - s_{jl}) + \frac{S}{N} \sum_{i \neq j} \sum_k \delta(t - \tau_{ik}), \quad (1b)$$

where $\delta(\cdot)$ is the Dirac delta function. The first term in Eq. (1b) corresponds to the currents arriving from the external input. Each neuron's external input is modeled by an independent Poisson train of current spikes with rate ν . At the l th spike time, $t = s_{jl}$, the j th neuron's voltage jumps by an amount f . The second term in Eq. (1b) corresponds to the currents arriving from within the network. At time τ_{jk} , when v_j reaches the threshold V_T , the j th neuron fires a spike. The voltage v_j is set to the reset voltage, which is assumed to be V_R here, and immediately becomes governed by Eq. (1a) again. At the same time, impulse currents are injected into all other neurons, increasing each neuron's voltage by an amount S/N . The scaling by N , the number of neurons in the network, ensures the average network input to any neuron remains bounded as $N \rightarrow \infty$.

We point out that in this model, a neuron's voltage is only increased at a time when it receives a spike from either the network or the external drive, and decays otherwise. Therefore, a neuron can only fire a spike at a time some neuron in the network receives a spike from the external drive.

In our model we incorporate an idealized refractory period by holding a neuron's voltage at the reset value after it has fired even if other neurons fire at the same time. This is in line with the discussion in [24], but prevents any neuron from firing more than once at any given time and thus the occurrence of bursts such as those described in [21–23].

In view of the properties described above, our numerical simulation method is event-driven, similar to the one discussed in Sec. 2.4.1 of [56]. This event-driven algorithm allows us to simulate our IF dynamics up to machine accuracy. We use the nondimensional values $g_L=1$, $V_R=0$, and $V_T=1$ in numerical simulations.

The effect on the network [Eq. (1a)] from an external Poisson spike train with rate ν and spike strength f is the same as from a constant current of strength $f\nu$ in the limit as $f \rightarrow 0$ and $\nu \rightarrow \infty$ while $f\nu \sim O(1)$. We will refer to this limit as the *zero-fluctuation limit*. Most results presented below are for the situation near this limit when f is small, and ν large,

with $f\nu \sim O(1)$, which we refer to as the *small-fluctuation regime*. As mentioned in the introduction, the zero-fluctuation limit for a single neuron also defines the *sub-threshold* regime, in which $f\nu < g_L(V_T - V_R)$, and the *super-threshold* regime, in which $f\nu > g_L(V_T - V_R)$.

III. SYNCHRONY

In the deterministic version of the pulse-coupled, all-to-all model (1), with constant external drive of strength $f\nu$, the evolution of the neuronal voltages is known to be rapidly attracted to a synchronous, time-periodic state [24]. In this state, all neuronal voltages evolve identically and produce periodic total firing events, during which all neurons fire at once, as already mentioned in Sec. I. The period $\hat{\tau}$ between two subsequent total firing events can be obtained exactly in terms of a single neuron's voltage, which is governed during this time by the equation $dv/dt = -g_L(v - V_R) + f\nu$ and satisfies the initial condition $v = V_R$ immediately after the first of the two firing events. In the superthreshold regime, it is easy to show that the period $\hat{\tau}$ satisfies

$$\hat{\tau} = \frac{1}{g_L} \ln \left(\frac{f\nu}{f\nu - g_L(V_T - V_R)} \right). \tag{2}$$

In the subthreshold regime, $f\nu < g_L(V_T - V_R)$, so the voltage never reaches V_T and no neuron in the network ever fires.

Under Poisson-train driving, for sufficiently large values of the Poisson rate ν and network coupling strength S , simulations of the network [Eq. (1)] reveal synchronous firing in a variety of forms. The raster plots shown in Fig. 1, where dots indicate which neuron fired at what time, show examples of synchronous dynamics of the network: partial synchrony [Fig. 1(a)], during which firing events occur that include a majority, but not all, of the network neurons; imperfect synchrony [Fig. 1(b)], during which firing events including all of the neurons are punctuated by occasional firings of individual neurons; and perfect synchrony [Fig. 1(c)], characterized by cascading total firing events during which all neurons fire in unison. Over a broad range of parameters in our simulations, not only does the network coupling sustain synchrony in the network dynamics, but it drives a network into a synchronous state. We note that the network coupling strength, while sufficiently large for achieving synchrony, is typically still weak in that it requires many incoming spikes from other neurons to cause a neuron to fire, that is, $S/N \ll V_T - V_R$.

We emphasize the tendency of the network [Eq. (1)] to synchronize over a broad range of parameters by plotting the average number of neurons firing instantaneously in a cascading event in Fig. 2. Complete asynchrony corresponds to an average of one neuron firing per cascade (black), while perfect synchrony corresponds to an average of all neurons firing in repeated total firing events (white). In both the sub-threshold (Fig. 2 top) and superthreshold (Fig. 2 bottom) driving regimes, the asynchronous dynamics are stable only in a very narrow region. Although cascades including half or a quarter of the network on average could still be considered synchronous dynamics, we will restrict ourselves to classifying

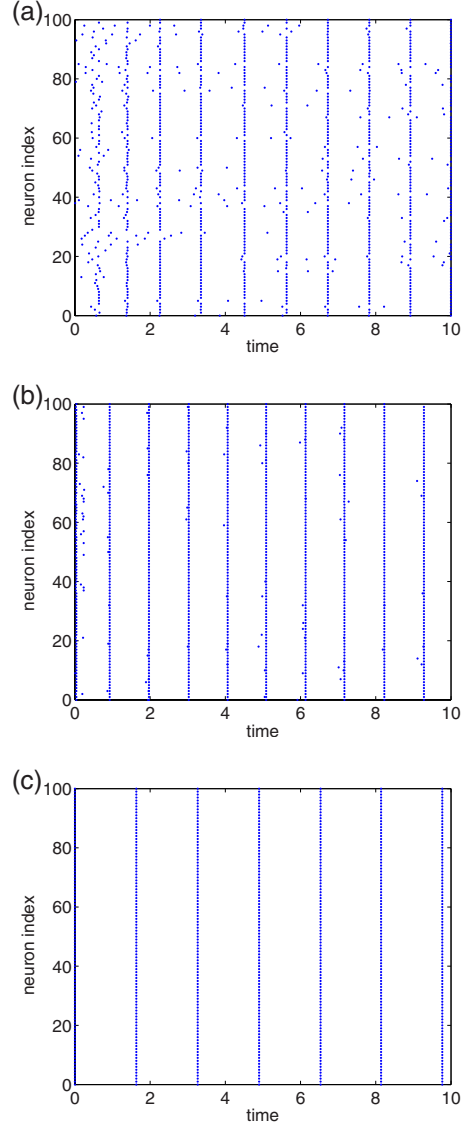


FIG. 1. (Color online) Raster plots of firing times for the system of $N=1000$ neurons (only 100 shown) with initial voltages chosen randomly between V_R and V_T . For the synchronizable network (c), with $f=0.0002$, $f\nu=1.2$ and $S=10.0$, one total firing event is followed by another total firing event with high probability, $P(C) = 0.952$. The other two systems, (a) with $f=0.01$, $f\nu=1.2$ and $S=0.5$, and (b) with $f=0.02$, $f\nu=1.2$, and $S=1.0$, do not satisfy our stringent definition of synchronizability.

ing synchrony in terms of cascading total firing events (white areas of Fig. 2) in the remainder of this paper.

As already mentioned in the introduction, the mechanism underlying the cascading total firing events in a Poisson-train-driven network differs from its deterministic counterpart in that individual neuronal trajectories are not identical and in fact spread apart between such events. Consequently, as we will see below, the average time between total firing events in the stochastically driven network is smaller than the period $\hat{\tau}$ given by Eq. (2), but approaches $\hat{\tau}$ as the fluctuations in the external driving current vanish.

During cascading total firing events, all neurons in the network fire simultaneously, and all neuronal voltages, v_j ,

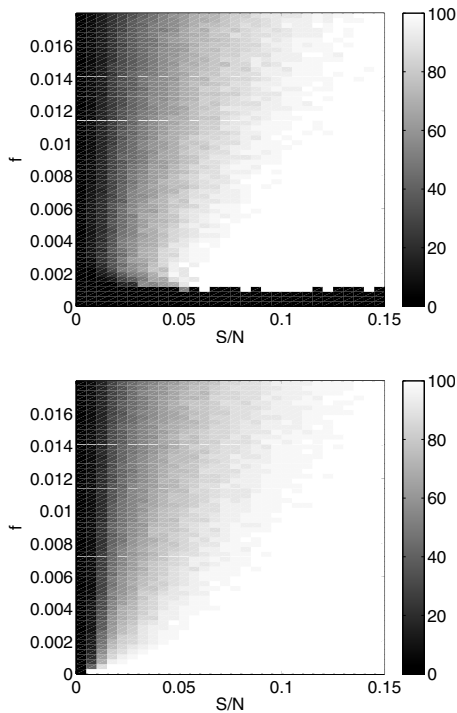


FIG. 2. Average cascade size per firing event as a function of spike strength, f , and coupling strength, S , for a network of $N = 100$ neurons with initial voltages chosen randomly between V_R and V_T . (top) Subthreshold regime, $f\nu=0.9$ and (bottom) superthreshold regime, $f\nu=1.2$. If no firing events were detected during the $t=400$ run, the cascade size was assigned to be zero.

are reset to V_R at the same time. The voltages then rise probabilistically, due to the stochastic external driving, until the first neuron fires and pushes all other neuron voltages upward and possibly above threshold. When the first neuron fires, the voltages of the remaining neurons are classified as *cascade-susceptible* if a total firing event ensues. We classify the network as *synchronizable* if the probability, $P(C)$, of neuronal voltages to be cascade-susceptible is sufficiently large. In the numerical examples presented below, we take the cutoff value to be $P(C)=0.85$. By this definition the networks (a) and (b) in Fig. 1 are not synchronizable, as other firing events frequently appear which are not part of the total firing events; they might be considered synchronous by some other less stringent characterization.

IV. SYNCHRONOUS FIRING RATE

In this section, we analyze the firing dynamics of the perfectly synchronous network. First, we study its mean firing rate in Sec. IV A using the probability density function (pdf) for the time between total firing events by relating it to the pdf of the time between firing events of a single uncoupled neuron. This analysis is carried out via a first-exit-time approach and is valid in both the subthreshold and superthreshold regimes. In Sec. IV B, we then use a central-limit argument to derive an approximate Gaussian pdf for the voltage of a neuron that has not yet fired. In addition to being important in its own right, the knowledge of this pdf also al-

lows for a particularly simple alternative method to obtain the mean time between total firing events in the superthreshold driving regime. The pdfs derived in this section will also be used later in Sec. V in computing the probability of finding repeated total firing events. The analysis in this section is based on the assumption that total firing events are seen in succession without extraneous neurons firing in between, so that the spiking rate of a neuron in the network is the inverse of the expected time between total firing events.

A. Distribution of the times between cascading total firing events

Here, we derive the firing rate of the network in terms of the firing rate of a single uncoupled neuron driven by a Poisson spike train with rate ν and spike strength f . In particular, since between cascading total firing events the neurons are effectively uncoupled, we can consider the N independent times that each of these neurons would take to spike if influenced by only its own external drive. We focus on the shortest of these times: the inverse of its average is used to obtain the network firing rate. In turn, the pdf for the spike time of a single uncoupled neuron is determined by solving the first-exit-time problem for the voltage crossing the firing threshold, V_T . As we will see below, in the small-fluctuation limit, this problem is described by a Fokker-Planck equation (FPE) with appropriate boundary conditions, which is solved analytically using an eigenfunction expansion.

We compute the pdf, $p_T^{(1)}(t)$, of the minimum exit time, $T^{(1)}$, of the N neurons in terms of the pdf, $p_T(t)$, of a single neuron's exit time (the time at which the neuronal voltage exits the domain $V_R \leq v < V_T$ through V_T) via the equation

$$p_T^{(1)}(t) = N p_T(t) [1 - F_T(t)]^{N-1}, \quad (3)$$

where $F_T(t) = \int_0^t p_T(t') dt'$ is the cumulative distribution function (cdf) of the exit time for a single neuron [57]. The expected time between total firing events is then deduced from Eq. (3) as

$$\langle T^{(1)} \rangle = \int_0^\infty t p_T^{(1)}(t) dt. \quad (4)$$

To approximate the single-neuron exit time distribution, $p_T(t)$, we remove the neuron from the system when its voltage reaches threshold, meaning that the neuron's voltage is "absorbed" at V_T rather than being reset back to V_R . Then, the probability that at time t this neuron has not yet fired (it will fire at a later time T) is the probability that it is still in the domain, $V_R \leq x < V_T$. This probability is

$$P(T \geq t) = 1 - F_T(t) = \int_{V_R}^{V_T} p_v(x, t) dx, \quad (5)$$

where x parameterizes the neuronal voltage whose pdf, $p_v(x, t)$, satisfies the Kolmogorov forward equation (KFE) for a single Poisson-spike-train-driven, IF neuron with an absorbing barrier at V_T [50,52,53,58,59]. The KFE may be thought of as expressing the conservation of probability density, and reads

$$\frac{\partial}{\partial t} p_v(x, t) = \frac{\partial}{\partial x} [g_L(x - V_R) p_v(x, t)] + \nu [p_v(x - f, t) - p_v(x, t)], \quad (6)$$

where incoming spikes are modeled by a Poisson spike train with rate ν and strength f .

A heuristic derivation of Eq. (6) proceeds as follows. The first term on the right-hand side of Eq. (6) represents the difference in the probability flux, $g_L(x - V_R)p_v(x, t)$, through the voltage values x and $x + dx$ due to the smooth streaming of phase points under the relaxation dynamics in Eq. (1a). The second term on the right-hand side of Eq. (6) reflects the fact that, with every incoming external spike, the neuron's voltage jumps by the amount f , and that these spikes arrive at the rate ν . A more detailed derivation of Eq. (6) can be found in [58]. Note that the pdf, $p_v(x, t)$, is defective in the sense that its integral over the domain $V_R \leq x < V_T$ does not equal unity for all times: the difference is exactly the probability that the neuron has reached threshold, V_T , and therefore been removed from further consideration.

A diffusion approximation to the KFE [Eq. (6)] can be obtained by considering f small, at least $f \ll V_T - V_R$, so that a large number of incoming spikes is needed to bring the neuronal voltage from reset to threshold. We Taylor expand the function $p_v(x - f, t)$ for small f , and keep the first three terms in this expansion, reducing Eq. (6) to the Fokker-Planck form

$$\frac{\partial}{\partial t} p_v(x, t) = \frac{\partial}{\partial x} \left[(g_L(x - V_R) - f\nu) p_v(x, t) + \frac{f^2 \nu}{2} \frac{\partial}{\partial x} p_v(x, t) \right]. \quad (7)$$

Here, the difference terms have been replaced by drift and diffusion terms. Note that the FPE [Eq. (7)] can be written in the conservation form

$$\frac{\partial}{\partial t} p_v(x, t) + \frac{\partial}{\partial x} J[p_v](x, t) = 0$$

with the probability flux $J[p_v](x, t)$ given by

$$J[p_v](x, t) = -(g_L(x - V_R) - f\nu) p_v(x, t) - \frac{f^2 \nu}{2} \frac{\partial}{\partial x} p_v(x, t). \quad (8)$$

The appropriate initial condition for Eq. (7) is

$$p_v(x, 0) = \delta(x - V_R), \quad (9)$$

as the neuronal voltage always starts at the reset voltage, V_R , after a total firing event.

The FPE [Eq. (7)] requires two boundary conditions. In particular, a reflecting boundary condition is imposed at $x = V_R$ because the actual neuronal voltage cannot dip below V_R , nor are any neuronal voltages injected into the network at $x = V_R$, due to the fact that firing neurons are removed from the system rather than having their voltages reset to V_R , as discussed above. This reflecting boundary condition requires the probability flux, $J[p_v](x, t)$, in Eq. (8) to vanish at $x = V_R$ [60,61],

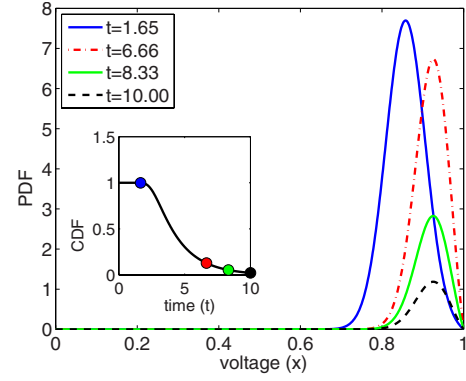


FIG. 3. (Color online) The relation between the probability, $P(T > t)$ in Eq. (5), of a single neuron to have not yet fired (inset) and the solution, $p_v(x, t)$, to the Fokker-Planck equation [Eq. (7)] at the indicated points in time with $f = 0.01$ and $f\nu = 0.95$.

$$J[p_v](V_R, t) = 0. \quad (10a)$$

In addition, the approximation that the neurons are removed from the network when their voltages reach the threshold V_T is encoded in the absorbing boundary condition at V_T :

$$p_v(V_T, t) = 0. \quad (10b)$$

Solving Eq. (7) with initial condition (9) and boundary conditions (10a) and (10b) is carried out in terms of an eigenfunction expansion involving confluent hypergeometric functions (see Appendix A for details). The dependence of the solution $p_v(x, t)$ on the voltage x for several moments of time t is depicted in Fig. 3. The probability that at time t the given neuron has not yet fired, $P(T \geq t)$, as calculated from $p_v(x, t)$ using Eq. (5), is shown in the inset.

From Eqs. (5), (7), (8), and (10a), we derive that the pdf of the first exit time is the flux of probability that leaves through the upper boundary [62,63],

$$p_T(t) = J[p_v](V_T, t). \quad (11)$$

The flux on the right-hand side can be calculated using the above-mentioned eigenfunction expansion to obtain $p_T(t)$, and the corresponding cdf, $F_T(t)$, is likewise calculated using Eq. (5), together yielding the pdf, $p_T^{(1)}(t)$, of the minimum exit time $T^{(1)}$ via Eq. (3). Equation (4) then gives the expected time between synchronous firing events, and the network firing rate is obtained as the inverse of this expected time.

While the above derivation of the firing rate in the perfectly synchronous regime of the network [Eq. (1)] is analytical, and both its main ingredients—the pdf and cdf of the first passage time of a single uncoupled neuron—are given in terms of eigenfunction expansions, the numerical evaluation of the expected minimum exit time $\langle T^{(1)} \rangle$ by this method can become difficult when its pdf is concentrated at small times. This is because, at these small times, the proximity to the delta function initial condition for the voltage pdf [Eq. (9)] calls for the evaluation of an excessive number of terms in the eigenfunction series. Moreover, each term in the eigenfunction series requires evaluating confluent hypergeometric functions at large values of their arguments where their

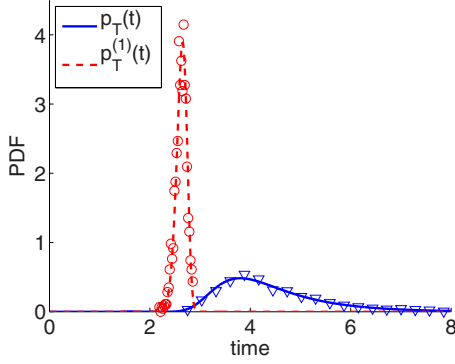


FIG. 4. (Color online) The pdf, $p_T(t)$, for the first exit time of a single, uncoupled, neuron (Eq. (11), solid line, blue online) and the pdf, $p_T^{(1)}(t)$, for the first exit time of $N=500$ neurons [Eq. (3), dashed line, red online] are compared to the results from 2000 numerical simulations of the single neuron and a network of 500 neurons (triangles and circles, respectively). The values $f=0.001$ and $f\nu=1.0$ are used.

power series representations converge poorly and various asymptotic representations need to be used instead. The initial condition (9) also makes solving Eq. (7) numerically difficult. Therefore, we present an alternative approach to obtain the pdf of the first exit time and solve it numerically.

To circumvent the convergence problems at small times associated with the delta-function initial condition (9), we consider an alternative equation describing the evolution of the function $G(x,t)$, the probability that a neuron's voltage has not yet crossed threshold given that it started at position x at time $t=0$. The cdf for the first exit time we are interested in, $F_T(t)$, is expressed as $F_T(t)=1-G(V_R,t)$. The function $G(x,t)$ satisfies the equation adjoint to the FPE [64]

$$\frac{\partial}{\partial t}G(x,t) = [-g_L(x-V_R) + f\nu]\frac{\partial}{\partial x}G(x,t) + \frac{f^2\nu}{2}\frac{\partial^2}{\partial x^2}G(x,t), \quad (12a)$$

with the boundary conditions

$$\frac{\partial}{\partial x}G(x,t)|_{x=V_R} = 0 \quad \text{and} \quad G(V_T,t) = 0. \quad (12b)$$

The initial condition for $G(x,t)$ is

$$G(x,0) = 1, \quad (12c)$$

in contrast to the delta-function initial condition for $p_v(x,t)$.

We solve the parabolic partial differential equation (12a) with the boundary and initial conditions (12b) and (12c) numerically with the Crank-Nicolson scheme [65]. We then compute the pdf $p_T(t)$ using a finite difference approximation for the derivative of the cdf $F_T(t)=1-G(V_R,t)$, both of which are then used to compute the pdf, $p_T^{(1)}(t)$, for the minimum exit time of all the N voltages via Eq. (3). The average of this time is then computed by integrating numerically the right-hand side of Eq. (4), and the network firing rate is again obtained as its inverse. Sample pdfs for $p_T(t)$ and $p_T^{(1)}(t)$ obtained in this way are shown in Fig. 4 which compare well

with the results obtained from the full numerical simulation of the original IF dynamics [Eq. (1)].

Results depicting the dependence of the network firing rate on the driving strength $f\nu$ are presented in Sec. IV C. The approximate theories described in this Section and Sec. IV B 2 are also verified against numerical simulations of the network [Eq. (1)].

B. Firing rate via average maximal voltage

The Fokker-Planck approximation (7) restricts us to consider the network dynamics in the small-fluctuation regime, $f \rightarrow 0$, $\nu \rightarrow \infty$, and $f\nu \sim O(1)$. In this regime, after a cascading total firing event during which all the neuronal voltages are reset to zero, it is natural to expect that the spread of the voltages stays small relative to their mean during the subsequent time evolution, and thus that the voltage dynamics can be described in a simple, explicit fashion. Here, we quantify such an approximation using a central-limit argument in which we neglect the reset upon crossing threshold V_T , and simply allow the neuronal voltages to evolve freely according to Eq. (1). Such an approximation is of course only appropriate until the first neuron fires again after a total firing event. In addition to being used in Sec. V for computing the probability of the network to be cascade-susceptible, this pdf also allows for a simple approximation to the time between total firing events that is valid in the superthreshold regime. In particular, in this regime, the time for the first neuron to cross threshold can be approximated by the time it takes the average maximal voltage to reach threshold, as described in Sec. IV B 2.

1. Gaussian approximation of voltage distribution

In this section, we describe how the pdf for a typical neuron voltage in the synchronized network evolves at times between total firing events. During these times, the voltage of each neuron can be expressed as a random sum, and in the small-fluctuation regime, we use a central-limit argument to show that their pdfs can be well approximated by independent Gaussian distributions. We outline the main steps here, and present the details in Appendix B.

When the network is in the perfectly synchronous state, no neurons fire during the time period between cascading total firing events, thus all the input to a given neuron is generated by the external spike train. Moreover, since the Poisson point process defining the incoming spike times, s_{jl} , has constant rate, the time can be reset to zero and the initial conditions $v_j(0)=V_R$, $j=1, \dots, N$, can be assigned after any total firing event. The solution to Eq. (1) during this time period is

$$v_j(t) = V_R + \sum_{l=1}^{M(t)} f e^{-g_L(t-s_{jl})}, \quad (13)$$

as we are not considering the reset mechanism when the voltage reaches threshold. The number, $M(t)$, of external spikes arriving at the j th neuron before the time t is random and Poisson distributed with mean νt . We remark that because the number $M(t)$ of terms in the sum in Eq. (13) is

random, the standard central-limit theorem does not directly apply to deriving the pdf of the voltage in Eq. (13) for large $M(t)$. Below we therefore construct a modification of the argument used to establish the central limit theorem, tailored to this random sum.

We restrict our discussion to the small-fluctuation regime and to times large compared to the inverse Poisson rate of the incoming external spike train, $1/\nu$. In this case, the voltage in Eq. (13) is a sum of a large, random number of independent random variables. Using a central-limit argument, we compute the cumulants of the corresponding voltage pdf and show in Appendix B that those of order 3 and higher are negligible for the voltage $v_j(t)$ in Eq. (13). This implies that, under the conditions $f \ll g_L(V_T - V_R)$ and $\nu \gg g_L$ while $f\nu \sim O(1)$, the pdf of the neuronal voltage, $v_j(t)$, which is not reset to V_R when it reaches threshold, is well approximated by the Gaussian distribution,

$$p_v(x,t) \sim \frac{1}{\sqrt{2\pi\sigma(t)}} \exp\left(-\frac{(x-\mu(t))^2}{2\sigma^2(t)}\right), \quad (14a)$$

with the average voltage

$$\mu(t) = V_R + \frac{f\nu}{g_L}(1 - e^{-g_L t}), \quad (14b)$$

and the voltage variance

$$\sigma^2(t) = \frac{f^2\nu}{2g_L}(1 - e^{-2g_L t}), \quad (14c)$$

both of which are derived in Appendix B. Note that, as time increases, both the mean and the variance of the voltage grow, as consistent with intuition, and asymptotically approach the values $V_R + f\nu/g_L$ and $f^2\nu/2g_L$, respectively. Later, the cdf of the voltage will also be needed, which is given by

$$F_v(x,t) \sim \frac{1}{2} \left[1 + \operatorname{erf}\left(\frac{x-\mu(t)}{\sqrt{2}\sigma(t)}\right) \right], \quad (14d)$$

where

$$\operatorname{erf}(z) = \frac{2}{\sqrt{\pi}} \int_0^z e^{-t^2} dt \quad (15)$$

is the error function. We compare the approximate voltage distribution in Eq. (14a) to that obtained from numerical simulation of the network [Eq. (1)] in Fig. 5.

2. Approximation for mean time between cascading total firing events

Using the approximate voltage distribution [Eq. (14a)], and the fact that the voltages of the neurons are effectively uncoupled and driven by independent spike trains between total firing events, we now calculate the average maximum

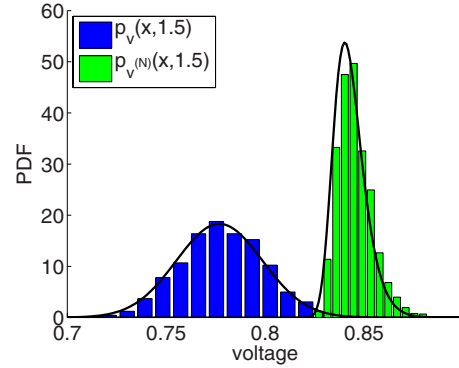


FIG. 5. (Color online) Gaussian approximation for the pdf, $p_v(x,t)$ in Eq. (14a), of the voltage of a typical neuron (dark gray, blue online), and the pdf, $p_v^{(N)}(x,t)$ in Eq. (16), of the maximum voltage of a set of $N=500$ neurons (gray, green online) at time $t = 1.5$, compared with results from Monte Carlo simulations of the network [Eq. (1)]. The values $f=0.001$ and $f\nu=1.0$ are used.

voltage from among these non-reset voltages at time t . The inverse of the time at which this average maximal voltage equals threshold is then used to approximate the firing rate of the synchronous network in the superthreshold regime. Note that this approach cannot be used in the subthreshold regime because the average maximum voltage may never reach threshold; the network firing in that regime is driven essentially by the voltage fluctuations.

For the synchronous network, the distribution of the maximal of the N voltages in the network is given by

$$p_v^{(N)}(x,t) = N p_v(x,t) F_v(x,t)^{N-1}. \quad (16)$$

In the superthreshold regime, in which the standard deviation of the maximal neuronal voltage is small in comparison to the mean of its distribution, the time τ when the first neuron crosses threshold can be approximated by the deterministic time it takes for the average of the maximal voltage to reach threshold, i.e.,

$$V_T = \int_{-\infty}^{\infty} x p_v^{(N)}(x, \tau) dx. \quad (17)$$

Solving Eq. (17) for τ , we obtain the firing rate of the network as τ^{-1} .

We can simplify the calculation of the time the first neuron crosses threshold considerably if we properly nondimensionalize Eq. (17). In particular, from Eqs. (14a) and (14d) it is clear that the maximal-voltage distribution, $p_v^{(N)}(x,t)$, in Eq. (16) can be written in terms of the normalized dimensionless variable

$$y = y(x,t) = \frac{x-\mu(t)}{\sigma(t)}. \quad (18)$$

Thus, we obtain $p_v^{(N)}(x,t) = g^{(N)}(y(x,t))/\sigma(t)$, with

$$g^{(N)}(y) = \frac{Ne^{-y^2/2}}{2^{N-1/2}\sqrt{\pi}} [1 + \operatorname{erf}(y/\sqrt{2})]^{N-1} \quad (19)$$

being the pdf for the maximal of N independent random variables distributed according to the standard Gaussian distribution. Equation (17) can now be rewritten as

$$V_T = \sigma(t)\mu_N + \mu(t), \quad (20)$$

$$\mu_N = \int_{-\infty}^{\infty} yg^{(N)}(y)dy \quad (21)$$

is now a universal quantity which only depends on the network size N . Using Eqs. (14b) and (14c), we can derive the explicit dependence of the time, τ_N , when the first of the N neurons crosses threshold, on μ_N , the external-drive spike strength f , and Poisson rate ν as

$$\tau_N = \frac{1}{g_L} \ln \left(\frac{f\nu(2\nu + g_L\mu_N^2)}{2\nu[f\nu - g_L(V_T - V_R)] + g_L\mu_N\sqrt{f^2\nu^2\mu_N^2 + 4f\nu^2(V_T - V_R) - 2g_L\nu(V_T - V_R)^2}} \right). \quad (22)$$

The value of μ_N in Eq. (21) can be obtained via numerical integration for each network size N ; its graph is shown in Fig. 6. The first neuron crossing time τ_N can then be obtained from Eq. (22). Note that in the zero-fluctuation limit, $f \rightarrow 0$, $f\nu = O(1)$, the time τ_N in Eq. (22) reduces to the deterministic oscillation period $\hat{\tau}$ in Eq. (2) as

$$\tau_N = \hat{\tau} - \frac{\mu_N\sqrt{(V_T - V_R)[2f\nu - g_L(V_T - V_R)]}}{\sqrt{2f\nu[f\nu - g_L(V_T - V_R)]}} \sqrt{f} + O(f). \quad (23)$$

Note also that the time τ_N approaches infinity as the driving strength $f\nu$ approaches the value

$$f\nu = g_L \left[V_T - V_R + \frac{1}{4}(f\mu_N^2 - \mu_N\sqrt{8f(V_T - V_R) + f^2\mu_N^2}) \right]$$

from above, for any given external-drive spike strength f and network size N . The term $g_L(V_T - V_R)$ corresponds to the zero-fluctuation limit, while the remaining terms give corrections for finite-size fluctuations.

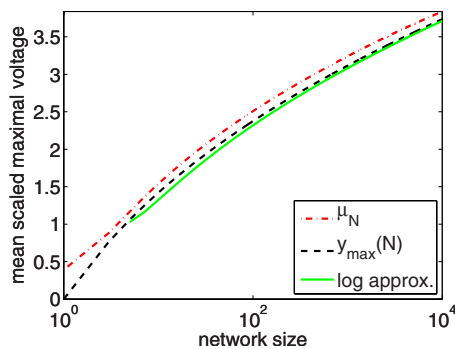


FIG. 6. (Color online) The dependence of the solutions μ_N in Eq. (21) (dash-dotted line, red online) and $y_{\max}(N)$ (dashed black line), along with its approximation in Eq. (24) (gray line, green online) on the network size, N . The approximation in Eq. (24) is derived assuming $N \gg 1$.

As an alternative to numerical integration of Eq. (21), since the pdf $g^{(N)}(y)$ in Eq. (19) is narrow for large network size N , we can approximate its mean μ_N by its mode, i.e., the value $y_{\max}(N)$ at which the pdf is maximized. The dependence of $y_{\max}(N)$ on the network size N can again only be obtained numerically (see Fig. 6). However, for large N , the value $y_{\max}(N)$ is well approximated by the expression

$$y_{\max}(N) \sim \sqrt{\ln \frac{N^2}{2\pi} - \ln \left(\ln \frac{N^2}{2\pi} \right)}. \quad (24)$$

The derivation of this asymptotic expression is given in Appendix C.

In Fig. 6, we present the plots of the quantities μ_N , $y_{\max}(N)$, and the asymptotic expression in Eq. (24) as functions of the network size N . They agree with each other reasonably well for $N > O(10)$. However, the curve $y_{\max}(N)$ and its approximation in Eq. (24) produce a slight undershoot. This is because the width of $g^{(N)}(y)$ scales only as $\sqrt{\ln N}$, so the approximation of its mean μ_N by its mode $y_{\max}(N)$ will have a logarithmically slowly decaying error. The network firing rates obtained using the approximations devised in this section will be discussed in the next section, where they will also be compared with the firing rates obtained using the more sophisticated first-passage-time method of Sec. IV A and those computed using numerical simulations.

C. Validity of firing-rate approximations

In this section, we discuss the results obtained from the two theoretical solutions discussed in Secs. IV A and IV B 2. These results are presented in the form of gain curves depicting the frequency of the synchronized oscillations (i.e., the average network firing rate) versus the average external current $f\nu$, shown in Fig. 7 along with the corresponding gain curves computed via numerical simulation of the network [Eq. (1)]. The comparison with the numerically computed gain curves is presented in order to check the validity of the assumptions used in the theoretical calculation of the firing rates.

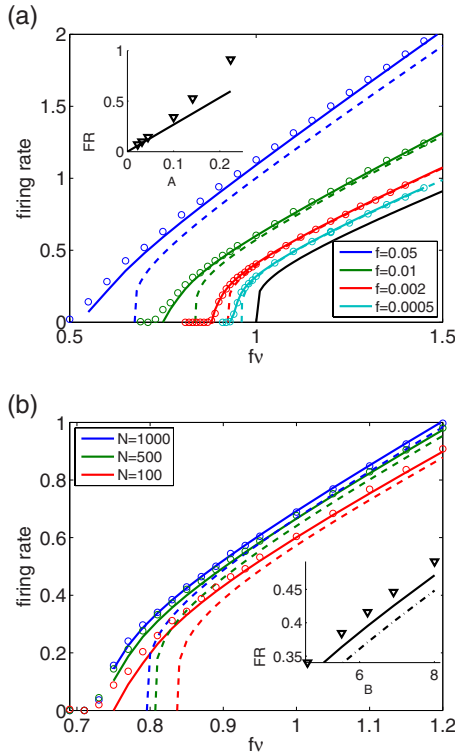


FIG. 7. (Color online) The firing rates determined by the methods in Sec. IV A (solid lines) and Sec. IV B (dashed lines) are compared with those obtained from numerical simulations (open circles) of the system [Eq. (1)] for 300 time units, as a function of $f\nu$. In (a) the gain curves for the indicated values of f while $N = 100$ and $S = 10$ show the synchronized stochastic network fires at a rate faster than $\hat{\tau}^{-1}$, the synchronized deterministic network firing rate in Eq. (2) (black line). In (b) the gain curves are plotted for the indicated values of N while $f = 0.01$ and $S = 20$. The inset in (a) compares the results of simulations (symbols) to the first term in the expansion of $1/\tau_N - 1/\hat{\tau}$ about $f = 0$, indicating a square root dependence of the firing rate, m , on the size of the fluctuations, f , for constant $f\nu = 1.20$, $N = 100$ and $S = 10$. The inset in (b) compares the results of simulations (symbols) to $1/\tau_N - 1/\hat{\tau}$ computed with μ_N from Eq. (21) (solid line) and $\mu_N = y_{\max}(N)$, using the approximation in Eq. (24) (dash-dot line), indicating a logarithmic dependence of the firing rate, m , on the size of the network, N , for constant $f\nu = 1.2$, $f = 0.01$, and $S = 20$.

As seen in Fig. 7(a), the synchronized network fires more frequently than a single neuron driven by a deterministic constant current [Eq. (2)], indicating a dependence on the size of the fluctuations of the neuronal voltages about the average network voltage. Both Figs. 7(a) and 7(b) indicate that the simpler maximal-voltage theory of Sec. IV B 2 describes the gain curves well in the superthreshold regime, but the more involved first-passage-time theory of Sec. IV A is needed to accurately describe the subthreshold regime, in particular, for larger values of f , i.e., larger fluctuations.

As either f , the strength of the external driving spikes, or N , the size of the network, increases, it becomes more likely to find one neuronal voltage further from the mean; this voltage reaches threshold faster and causes a total firing event. To understand the dependence of spike rate, m , on f and N , we first note that the size of the standard deviation, the

square root of the expression in Eq. (14c), of the voltage pdf $p_v(x, t)$ scales as \sqrt{f} for fixed $f\nu$. Decreasing f within the small-fluctuation regime tightens the pdf $p_v(x, t)$ of the neuronal voltages, thereby extending the amount of time needed for some neuron to reach threshold, and slowing the firing rate. We obtain this same scaling for $m - 1/\hat{\tau}$, where $\hat{\tau}$ is the deterministic oscillation period in Eq. (2), by taking $m = 1/\tau_N$ from Eq. (22) and using the expansion in Eq. (23). The size of the network N has a weaker effect on the firing rate since the typical deviation of the maximal neuronal voltage from the mean neuronal voltage in a population of N neurons grows approximately logarithmically with N . This is seen through the large- N (i.e., large- μ_N) asymptotics of Eq. (22), which give $m \sim f^2 \nu \mu_N^2 / (V_T - V_R)^2 + O(1)$, and replacing the mean μ_N by the expression in Eq. (24). We have verified through full simulations of system [Eq. (1)] that the firing rate depends on the square root of the spike strength f for small f near the deterministic oscillation period $\hat{\tau}$, and logarithmically on the network size N for large N , under fixed superthreshold external driving strength $f\nu$, as shown in the insets in Fig. 7.

V. PROBABILITY TO BE CASCADE-SUSCEPTIBLE

In this section, we investigate in which parameter regimes the neuronal network [Eq. (1)] exhibits perfect synchronous behavior, manifested through cascading total firing events. As we recall from Secs. III and IV, during such an event, the firing of one neuron causes all subsequent neurons to fire in immediate succession. To determine if the network is expected to exhibit this type of synchrony, we follow the evolution of neuronal voltages initially set at the reset value V_R , and compute the probability that, when the first neuron fires, all the other neurons are in a configuration that allows for a cascading total firing event. This is precisely the probability for the network to be *cascade-susceptible*. We further investigate this probability in situations when additional physiological effects that can impede or break synchrony are incorporated into the model.

A. Theoretical calculation

A cascading total firing event occurs if, for any given neuron, the total input current from neurons with greater voltage, firing previously in the cascade-firing event, is sufficiently large to bring this neuron's voltage above threshold, and therefore fire. In other words, the cascade-firing event is being perpetuated until all neurons fire. If we order the neuronal voltages so that $V^{(k)} > V^{(j)}$ for $k > j$ at the time the first neuron fires, $T^{(1)}$, then the above consideration can be summarized as an intersection of events in the *cascade-susceptibility condition*

$$C = \bigcap_{k=1}^{N-1} C_k, \tag{25}$$

where C_k denotes the event

$$C_k: V_T - V^{(k)} \leq (N-k) \frac{S}{N}, \quad (26)$$

with S being the coupling strength among the N neurons in the network. The probability $P(C)$ of the event C is computed in terms of the distribution of the neuronal voltages.

We compute the probability of condition (25) being satisfied by integrating over the conditional probability of the random time $T^{(1)}$ at which the first neuron fires,

$$P(C) = \int_0^\infty P(C|T^{(1)} = t) p_T^{(1)}(t) dt. \quad (27)$$

Here, the pdf for the exit time of the first of N neurons, $p_T^{(1)}(t)$, is given in Eq. (3). We simplify the computation by approximating the conditional probability distribution in the integrand of Eq. (27) as if each neuronal voltage were independently distributed according to its freely evolving (without reset) probability distribution $p_v(\cdot, t)$ evaluated at the specified time t , subject to the condition that the neuron with maximum voltage is at that moment of time exactly at threshold,

$$P(C|T^{(1)} = t) \approx P(C|V^{(N)}(t) = V_T). \quad (28)$$

The conditions expressed on the two sides of Eq. (28) are not quite equivalent because the condition $T^{(1)} = t$ implies also that no neuron's voltage ever reached threshold before time t , whereas the approximating condition $V^{(N)}(t) = V_T$ makes no reference to the properties of the voltages at times previous to t . The error in this approximation is expected to be small because the neuronal voltages are rising on average so the condition that the neuron with maximal voltage is at threshold at the end of the interval $[0, t]$ makes it rather unlikely that any of the neurons crossed threshold much earlier.

Under the approximation in Eq. (28), in the small-fluctuation regime, we use the Gaussian approximation (14a) for the freely evolving single-neuron voltage distribution, truncated at V_R and V_T and renormalized to unit integral over the voltage interval $V_R < x < V_T$, to obtain the pdf of the voltages for the neurons which have not yet fired at time t ,

$$\tilde{p}_v(x, t) = \frac{p_v(x, t)}{\int_{V_R}^{V_T} p_v(x', t) dx'}, \quad V_R < x < V_T. \quad (29)$$

The accuracy of the approximation in Eq. (28) was verified by measuring the distance between the proposed theoretical cdf derived from the pdf in Eq. (29) and the sample cdf taken from full numerical simulations of the system [Eq. (1)] using the Kolmogorov-Smirnoff test (with significance level $\alpha = 0.05$).

To compute the conditional probability in Eq. (27) we will instead subtract from unity the probability of the complement of event C , i.e., the probability that the firing event fails to include all neurons, which is easier to compute explicitly. The cascade-susceptibility condition (25) is not fulfilled if it contains at least one value of k for which condition (26) fails. We divide up the complement of event C into the mu-

tually exclusive events A_j , each requiring condition (26) to be satisfied for $k=N-1$ to $k=N-j+1$ and to have failed for $k=N-j$. The total probability of cascade failure is the sum of the probabilities to fail first at each step,

$$P(C|V^{(N)}(t) = V_T) = 1 - \sum_{j=1}^{N-1} P(A_j|V^{(N)}(t) = V_T). \quad (30)$$

To determine the probability of event A_j , we divide the voltage interval $V_R \leq x \leq V_T$ into bins of width S/N starting at V_T , so that the first bin is $V_T - S/N < x \leq V_T$. The probability $p_k(t)$ for a neuron's voltage to be in the k th bin is given by the formula

$$p_k(t) = \int_{V_T - kS/N}^{V_T - (k-1)S/N} \tilde{p}_v(x, t) dx, \quad (31)$$

with the pdf $\tilde{p}_v(x, t)$ as in Eq. (29). For the cascade to fail precisely at the j th neuron, one neuronal voltage must be in the first bin, two in the first two bins, three in the first three bins, and so forth, until $j-1$ are in the first $j-1$ st bins, none are in the j th bin, and the remainder fall below the j th bin. We sum over all configurations of the unordered neuronal voltages consistent with this description of event A_j , resulting in

$$P(A_j|V^{(N)}(t) = V_T) = \sum \frac{(N-1)!}{n_1! n_2! \dots n_{j-1}! (N-j)!} p_1(t)^{n_1} \times p_2(t)^{n_2} \dots p_{j-1}(t)^{n_{j-1}} \left[1 - \sum_{i=1}^j p_i(t) \right]^{N-j} \quad (32)$$

where n_k denotes the number of neurons with voltage in the k th bin, $\sum_{k=1}^{j-1} n_k = j-1$, and p_k is defined in Eq. (31).

The remaining problem is to evaluate the terms in Eq. (30) since enumerating the configurations of neuronal voltages is time consuming for large j . The first few terms dominate this sum, as simulations show that the cascading event is very unlikely to fail after the first four or five neurons fire. When evaluating the probability $P(C)$, the sum in Eq. (30) is terminated when terms are less than 10^{-4} . With this tolerance, two to nine terms are included depending on the parameter values. In the next section, we compare this method of computing $P(C)$ to the result of direct numerical simulations and discuss the dependence on the network parameters.

B. Parameter dependence of synchrony

The previous section analyzed a mechanism for the network [Eq. (1)] to maintain a self-consistent state of synchrony by calculating the probability to see repeated cascading total firing events. Using numerical simulations, we calculate the probability to be cascade-susceptible by repeatedly starting all neurons at reset voltage, which is the state after a previous cascading total firing event, and simulating the network dynamics until the first neuron fires; the probability to be cascade-susceptible is the fraction of the total number of simulations represented by those that lead to the firing of all N neurons in the network. The theoretical char-

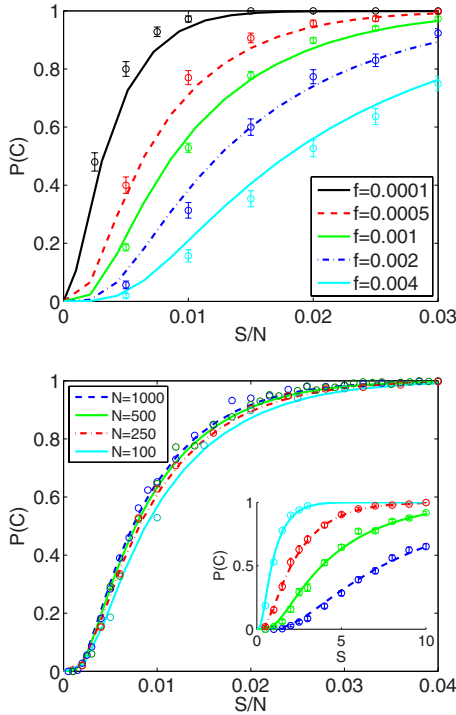


FIG. 8. (Color online) Probability that condition (25) holds, $P(C)$, vs network coupling strength scaled by network size, S/N , computed with the method in Sec. V A (lines) and from numerical Monte Carlo simulation of system (1) (symbols), averaged over 500 simulations. Top: for the indicated values of f , $N=100$ and $f\nu = 1.2$. Bottom: for the indicated values of N , $f\nu=1.2$ and $f=0.001$. Inset: same data plotted vs S .

acterization, $P(C)$ as discussed in Sec. V A, of the network synchronizability in terms of its governing parameters agrees well with results from numerical simulations, as illustrated in Fig. 8, and therefore allows for a quantitative analysis of how the network synchrony depends on the model parameters, f , N , S , and $f\nu$.

The synchronizability as characterized by $P(C)$ has smooth dependence on parameters (Figs. 8 and 9). The system becomes more synchronizable as $P(C)$ becomes steeper for smaller spike strength f with the driving strength $f\nu$ held constant. Larger values of f correspond to larger fluctuations spreading the neuronal voltages apart, requiring larger network coupling strengths for the cascade-susceptibility condition (25) to hold with high probability. From Fig. 8, the synchronizability appears to depend at most weakly on the network size N , apart from the dependence on the scaled coupling strength S/N .

The network becomes less synchronizable for subthreshold driving (Fig. 9). As the average neuronal voltages fall further below threshold, it is less likely a neuronal voltage is S/N from threshold when the first neuron fires, thus it is less likely for the cascading event to begin. The smooth parameter dependence of the synchronizability characterized by $P(C)$ develops a sharp transition which approaches a threshold, $f\nu=1$, as the fluctuations decrease, i.e., f decreases for fixed $f\nu$. The network in the zero-fluctuation regime, in which all the neurons in the network are driven with constant current of strength $f\nu$, would have a sharp transition at

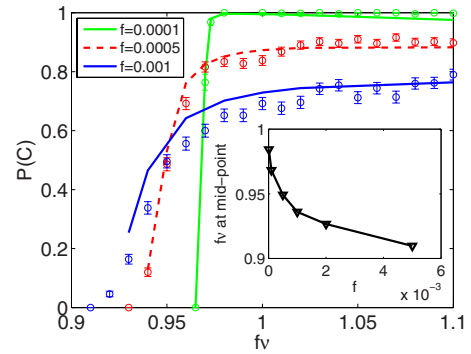


FIG. 9. (Color online) Probability that condition (25) holds, $P(C)$, vs mean external current, $f\nu$, computed with the method in Sec. V A (solid lines) and from Monte Carlo numerical simulation of system (1) (symbols), averaged over 500 samples. For each curve with the indicated values of f , $N=100$ and $S=1.5$. Inset: Value of $f\nu$ at the location of the transition [where $P(C)=0.5$] between asynchronous and synchronous behavior as a function of fluctuation size, f .

$f\nu=1$ from no firing [$P(C)=0$] to synchronous firing [$P(C)=1$], as depicted in the inset of Fig. 9.

C. Additional physiological effects

A number of physiological effects as yet not included in the model (1) are likely to reduce the probability of total firing events or eliminate them altogether. These effects include network sparsity, synaptic failure, random transmission delays, and finite current rise and decay times. We add them one at a time to the model and investigate how they affect the synchrony by comparing corresponding raster plots qualitatively and calculating the probability to be cascade-susceptible both theoretically and from numerical simulations.

Spikes from one neuron in the network are prevented from affecting another neuron in two possible ways: permanently, if no synaptic connection exists between the two neurons, or occasionally, if the synaptic transmission fails at random. To model the first case, we construct a random sparse network from an all-to-all coupled network by removing each connection independently with probability p_c . Thus, a single neuron will be connected to $(1-p_c)N$ other neurons on average. We take $1-p_c$ sufficiently large so that the network is likely to have only one connected component, otherwise a total firing event would be impossible. The second case, random synaptic transmission failure, is modeled by preventing each spike within the network from reaching any one of its target neurons with probability p_f . This is done by replacing the current driving the j th neuron in Eq. (1b) with a current of the form

$$I_j(t) = f \sum_l \delta(t - s_{jl}) + \frac{S}{N} \sum_{i \neq j} \sum_k \rho_{jik} \delta(t - \tau_{ik}),$$

where $\rho_{jik}=0$ with probability p_f , and 1 with probability $1-p_f$. In effect, each neuron behaves as though it is connected to $(1-p_f)N$ other neurons on average. In both cases, the number of input spikes a neuron receives from the other

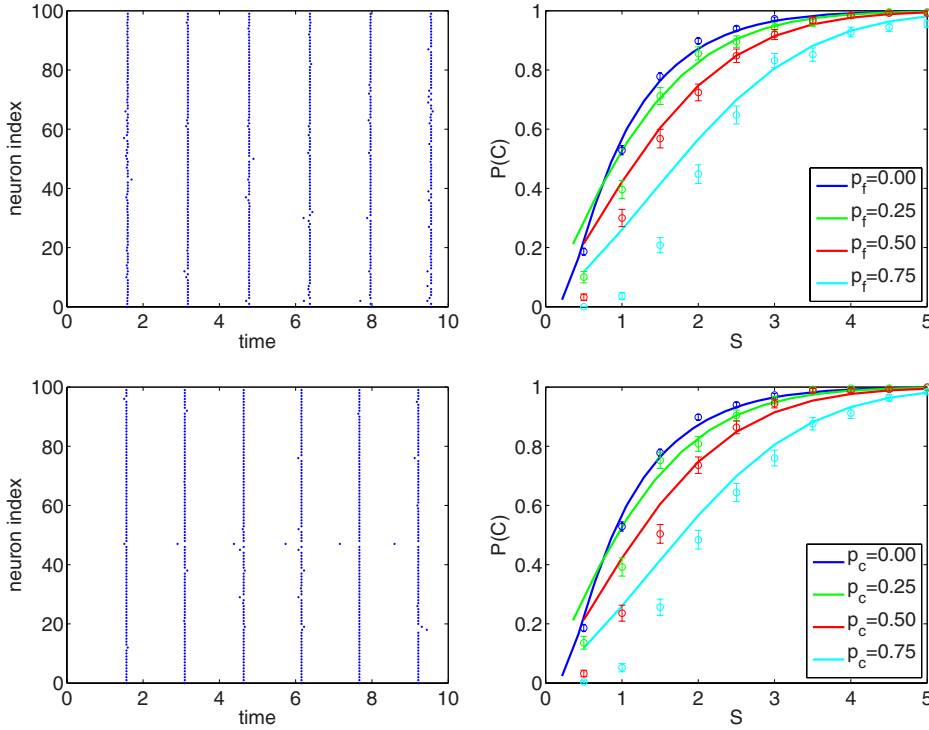


FIG. 10. (Color online) Behavior of the network [Eq. (1)] with the addition of (top) synaptic failure and (bottom) sparse random network connections. Theoretical computation with modification to Eq. (30) (solid lines) is compared to results from numerical Monte Carlo simulations (circles with error bars), averaged over 500 simulations and (bottom) 10 networks. The values $f=0.001$, $f\nu=1.2$, $S=2.0$, and (right) the indicated values of p_f and p_c , (top left) $p_f=0.90$, (bottom left) $p_c=0.90$ are used.

neurons in the network is reduced. In statistical mechanics terms, synaptic failure is an annealed disorder in which the randomness of connections between neurons keeps fluctuating, while the random sparsity in the network is a quenched disorder as the randomness of connections between neurons is frozen from the start of the simulation.

Synaptic failure and network sparsity affect the probability to be cascade-susceptible in a statistically identical fashion. The transition from synchronous to asynchronous behavior remains smooth as either p_f or p_c is increased (Fig. 10). We implement a rough modification for our theoretical calculation of $P(C)$ to account for either. When considering the arrangement of the subthreshold neurons, not only must condition (26) be satisfied for appropriate values of k , but the neuron must receive each spike either by being connected to the spiking neuron (with probability $1-p_c$) or having successful transmission (with probability $1-p_f$). We modify the calculation of $P(C)$ by multiplying the voltage distribution given in Eq. (29) used in calculating $P(A_j|V^{(N)}(t)=V_T)$ in Eq. (30) by either $1-p_c$ or $1-p_f$. This modification is rather crude, in that each neuron is assumed to receive or not receive every potential incoming spike according to whether or not it received the first potential incoming spike. Still, this agrees approximately with the results from numerical simulations (Fig. 10). Unlike in the discrete model discussed in [66], we do not see the persistence of both a synchronous and asynchronous state for the same parameter values.

Although both synaptic failure and network sparsity are equally effective at reducing synchrony in terms of the probability to be cascade-susceptible, neither is effective at completely removing the coherent structure of cascading events with many neurons in the network firing at the same time, as shown in the raster plots in Fig. 10. These cascading events are a product of the instantaneous coupling between the neurons in the network, and can be eliminated by adding random

delay times to the transmission of spikes, or by incorporating finite rise and decay times in the synaptic current model, effectively imposing a transmission delay.

Random delays between the time a neuron spikes and the times the other neurons in the network receive these spikes, modeling the variable speed of transmission or axon length [67–69], can be described by replacing the current in Eq. (1b) with

$$I_j(t) = f \sum_l \delta(t - s_{jl}) + \frac{S}{N} \sum_{i \neq j} \sum_k \delta(t - \tau_{ik} - T_{jik}), \quad (33)$$

where each T_{jik} is a non-negative random variable. For simplicity, we take T_{jik} to be exponentially distributed with common mean.

Incorporating finite current rise and decay times in the network [Eq. (1)] amounts to replacing the instantaneous, delta-function currents in Eq. (1b) by α -function type currents, where we take

$$\alpha(t) = \Theta(t) \frac{t}{\tau_E} e^{-t/\tau_E}, \quad (34)$$

with τ_E being the decay time and $\Theta(t)$ the Heaviside function. (The rise time is defined as the time when $\alpha(t)$ reaches its maximum.) As the model currents are now continuous in time, a neuron can spike at times later than those at which it receives spikes. Thus, while the differential equation (1a) with this type of continuous current can still be solved explicitly, the spike times must be found numerically. Alternatively, we numerically simulate the network [Eq. (1a)] with the delta-function currents in Eq. (1b) replaced by α -type currents [Eq. (34)], using a modified version of the algorithm developed in [70].

Networks with synaptic transmission delays are always asynchronous by our definition (Fig. 11), as transmission de-

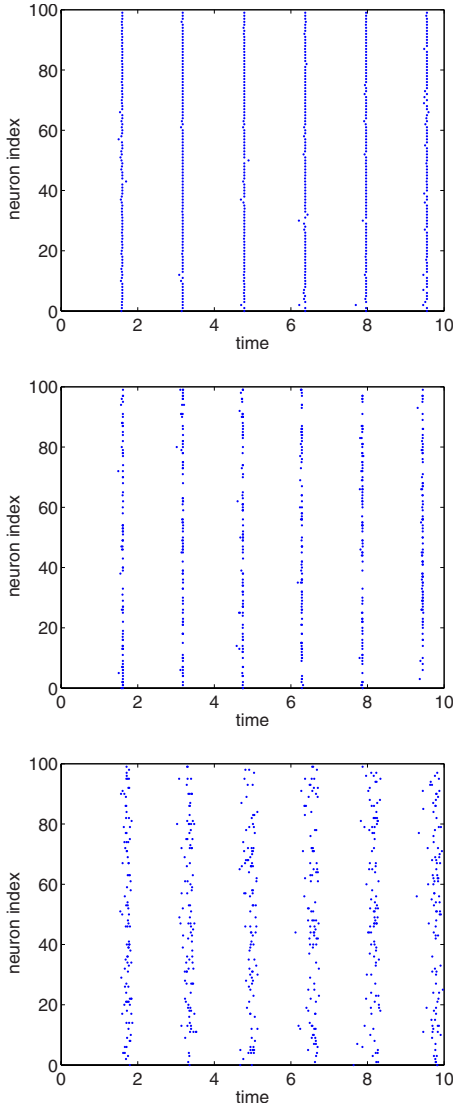


FIG. 11. (Color online) Raster plots demonstrating the behavior of the network with random transmission delay. $N=100$, $f=0.001$, $f\nu=1.2$, $S=0.1$; (top) no delay (middle) average delay 0.002 (bottom) average delay 0.2

lays make total firing events impossible [$P(C)=0$]. However, the firing of the network is still synchronous in a broader sense as there are smaller intervals of high firing rate and larger intervals during which no neurons fire. A relatively large delay time relative to the time between the periods of high firing rate is needed to completely desynchronize the network.

Finite current rise times effectively act as (fixed) synaptic delay times since, upon receiving a spike, a neuron’s voltage does not increase instantaneously and so a neuron is not likely to spike immediately. Therefore, synchronous total firing events are again impossible (Fig. 12) in networks incorporating finite current rise and decay times, and thus $P(C)=0$. Similarly to the random delay times, this network with finite current rise times maintains synchrony in a broader sense as described in the preceding paragraph. Long rise and decay times are needed to completely eliminate this broader synchronous firing.

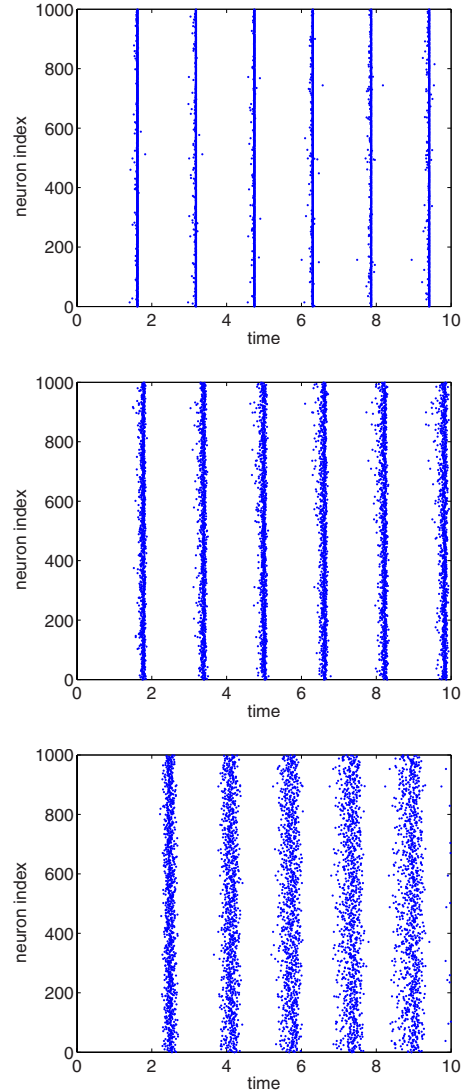


FIG. 12. (Color online) Raster plots for the network with the delta functions in Eq. (1b) replaced by $t^2/\tau_E^2 \exp(-t/\tau_E)$. $N=1000$, $f=0.001$, $f\nu=1.2$, $S=0.1$; (top) $\tau_E=3 \times 10^{-6}$ (middle) $\tau_E=3 \times 10^{-2}$ (bottom) $\tau_E=3 \times 10^{-1}$

VI. CONCLUSIONS

Oscillatory dynamics involving cascading total firing events in Poisson-train-driven, all-to-all coupled, excitatory, integrate-and-fire neuronal networks with instantaneous spiking appear to be natural attracting states of such networks, at least in the small-fluctuation regime [66,71]. Our own numerical simulations have confirmed that the basin of attraction for such oscillatory dynamics is quite large, unlike for the asynchronous dynamics, for which this basin becomes smaller and smaller as the size of the external-drive fluctuations decreases [58,71]. As we show in Sec. V B, the sharp threshold separating no firing in the subthreshold driving case and periodic cascading total firing events in the superthreshold driving case, which exists when the external driving is deterministic [24], gives way to a continuous probability distribution of total firing events, depending on the external driving strength and other network parameters, when the network is Poisson-train-driven.

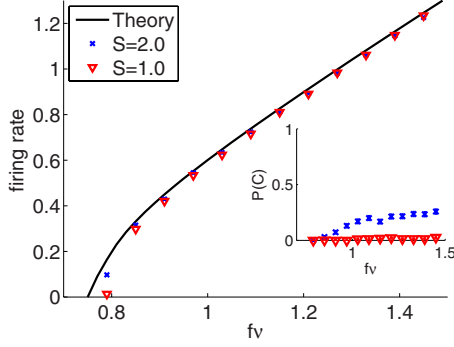


FIG. 13. (Color online) Gain curve comparison between the theory (solid line) derived in Sec. IV A and full numerical simulations of the system [Eq. (1)] (symbols) when $P(C) < 0.85$, our cutoff for classifying the network as synchronous. For the two values of internal coupling, we keep $N=100$ and $f=0.001$ constant. Inset: the value of $P(C)$ obtained from Monte Carlo numerical simulations (500 samples) for both values of S as a function of $f\nu$.

The notion of synchronizability as defined in this work and with it the probability $P(C)$ of a network to be cascade-susceptible are rather stringent in requiring all neurons to fire together in cascading total firing events. In particular, the assumption of infinitely short and instantaneously transmitted spikes is crucial for the perfect synchrony described here, and thus also the relevance of the probability $P(C)$. As we have seen in Sec. V C, the inclusion of either delay times or finite current rise times immediately destroys perfect synchrony. Nevertheless, a statistical type of synchrony survives provided these times are not too long, and a proper statistical description of it is a challenging open problem. Our firing-rate approximations developed in Secs. IV A and IV B 2 should still be at least approximately applicable under the conditions of imperfect synchrony when a few neurons fire out of step (Fig. 13).

The work presented in this paper was in part motivated by the desire to understand the attractor states of different IF-type neuronal networks. For all-to-all coupled Hodgkin-Huxley networks, three types of attractor states were found numerically using a generalization of Lyapunov exponents for dynamical systems with discontinuities: periodic, chaotic, and quasiperiodic [72,73]. If IF-type systems are to give truly useful approximate descriptions of neuronal-network dynamics, they should be able to reproduce the same dynamical regimes. That this is indeed the case was confirmed for all-to-all coupled conductance-based IF networks with finite conductance rise and decay times [74]. On the other hand, the model network with instantaneous response discussed here cannot exhibit chaotic dynamics [58]. The discussion in Sec. III shows that spike-to-spike synchrony via total firing events appears to be one of the prevalent attracting states of the network even under random, Poisson-train external drive. This is one of the reasons why we have undertaken a thorough, analytical investigation of this synchrony.

The network dynamics we have discussed in this paper could be modified to include a highly idealized, instantaneous version of the bursts that occur in all-excitatory networks, as described in [19–23]. This modification would

consist of allowing a neuron's voltage to jump up in the course of a cascading firing event even after this neuron has fired. Thus, every neuron would have the potential to spike several, if not infinitely many, times during one such an event. The resulting instantaneous bursts could therefore in principle contain infinitely many spikes; for this not to happen, one should include refractory effects such as synaptic depression consisting of either an increased probability of transmission failure or some attenuation mechanism for the size of voltage jumps due to a spike as the burst proceeds.

Finally, in Sec. V C we also addressed the question of how network architecture affects perfect synchrony in the case of a sparse network with randomly chosen missing interneuronal connections. For more general network architecture types, this question is still open. We are in the process of addressing it in the case of scale-free networks [75].

ACKNOWLEDGMENTS

K.A.N. was supported by NSF Grant No. DMS-0636358. G.K. was partly supported by NSF Grant No. DMS-0506287. P.R.K. was partly supported by NSF Grant No. DMS-0449717. D.C. was partly supported by NSF Grants No. DMS-0506396, No. DMS-0507901, and No. DMS-1009575, and a grant from the Swartz Foundation.

APPENDIX A: SOLUTION TO THE FPE

To solve Eq. (7), we develop a series expansion of the form [64]

$$p_\nu(x,t) = p_s(x) \sum_{n=0}^{\infty} A_n Q_n(x) e^{-\lambda_n t}, \quad (\text{A1})$$

where $Q_n(x)$ and λ_n are the eigenfunctions and eigenvalues of the adjoint problem

$$\left[-g_L(x - V_R) + f\nu \right] \frac{d}{dx} Q_n(x) + \frac{f^2 \nu}{2} \frac{d^2}{dx^2} Q_n(x) + \lambda_n Q_n(x) = 0, \quad (\text{A2a})$$

with boundary conditions

$$\frac{d}{dx} Q_n(x) \Big|_{x=V_R} = 0 \quad (\text{A2b})$$

and

$$Q_n(V_T) = 0. \quad (\text{A2c})$$

The function

$$p_s(x) = \exp\left(-\frac{(g_L(x - V_R) - f\nu)^2}{f^2 \nu g_L} \right) \quad (\text{A3})$$

is the stationary solution for the related problem of Eq. (7) but with reflecting boundary conditions at both ends (zero flux). The constants A_n are determined from the initial condition (9) via the equation

$$\int_{V_R}^{V_T} \delta(x - V_R) Q_n(x) dx = A_n \int_{V_R}^{V_T} p_s(x) Q_n^2(x) dx,$$

for which the δ -function resides inside the interval, as it represents the initial probability density and must integrate to unity, so that

$$A_n = \frac{Q_n(V_R)}{\int_{V_R}^{V_T} p_s(x) Q_n^2(x) dx}. \quad (\text{A4})$$

The solution to Eq. (A2a) is obtained through two transformations of variables. First, we shift and rescale the variable x so that

$$z = \frac{g_L(x - V_R) - f\nu}{f\sqrt{g_L\nu}}.$$

The system is now driven to $z=0$ by the average drift, and has essentially been rescaled by the standard deviation, which is $O(f\sqrt{\nu})$. Taking another transformation, $\zeta = z^2$, Eq. (A2a) for $Q_n(x)$ becomes the equation for the transformed solution $\hat{Q}_n(\zeta)$,

$$\zeta \hat{Q}_n''(\zeta) + \left(\frac{1}{2} - \zeta\right) \hat{Q}_n'(\zeta) + \frac{\lambda_n}{2g_L} \hat{Q}_n(\zeta) = 0, \quad (\text{A5})$$

where $Q_n(x) = \hat{Q}_n(\zeta(z(x)))$.

Equation (A5) is a subcase of the confluent hypergeometric equation

$$\xi \frac{d^2 w(\xi)}{d\xi^2} + (b - \xi) \frac{dw(\xi)}{d\xi} - aw(\xi) = 0. \quad (\text{A6})$$

Its solutions are linear combinations of the Kummer function [76],

$${}_1F_1(a, b, \xi) = \sum_{n=0}^{\infty} \frac{(a)_n \xi^n}{(b)_n n!}, \quad (\text{A7a})$$

and either

$$\xi^{1-b} {}_1F_1(1 - a, 2 - b, \xi) \quad (\text{A7b})$$

or the associated Kummer function

$$U(a, b, \xi) = \frac{\pi}{\sin \pi b} \left[\frac{{}_1F_1(b - a, b, \xi)}{\Gamma(1 + a - b)\Gamma(b)} - \frac{\xi^{1-b} {}_1F_1(1 - a, 2 - b, \xi)}{\Gamma(a)\Gamma(2 - b)} \right]. \quad (\text{A7c})$$

Here $(c)_0 = 1$, $(c)_n = c(c+1)(c+2)\dots(c+n-1)$ is the Pochhammer symbol [77].

For our Eq. (A2), the first solution in terms of the variable z , where the replacement $\zeta = z^2$ has been made, is

$${}_1F_1\left(-\frac{\lambda_n}{2g_L}, \frac{1}{2}, z^2\right). \quad (\text{A8a})$$

The second linearly independent solution can be written as either

$$|z| {}_1F_1\left(-\frac{\lambda_n}{2g_L} + \frac{1}{2}, \frac{3}{2}, z^2\right) \quad (\text{A8b})$$

or

$$U\left(-\frac{\lambda_n}{2g_L}, \frac{1}{2}, z^2\right). \quad (\text{A8c})$$

We choose those forms of the second solution at different stages of the calculation to best reduce numerical error.

The two functions in formulas (A8b) and (A8c) are not smooth at $z=0$ because the mapping of $z \rightarrow \zeta$ is 2-1 rather than 1-1. Since the solutions, $\hat{Q}(\zeta(z))$, must be continuously differentiable at $z=0$, two different linear combinations must be taken for $z > 0$ and $z < 0$, with function and derivative matching at $z=0$. The resulting 4×4 system of equations for determining the eigenvalues reduces to a single equation,

$$\phi_1(\lambda_n) + \phi_2(\lambda_n) = 0, \quad (\text{A9})$$

where for any given basis of $y_1(z)$ from Eq. (A8a) and $y_2(z)$ chosen from Eqs. (A8b) and (A8c), we define $\phi_1(\lambda_n) = [dy_2(z_R)/dz]/[dy_1(z_R)/dz]$ and $\phi_2(\lambda_n) = y_2(z_T)/y_1(z_T)$. Equation (A9) is solved numerically for the eigenvalues, λ_n . The solution, $p_v(x, t)$, to Eq. (7) is obtained by numerically evaluating a sufficiently large number of terms in Eq. (A1).

APPENDIX B: CUMULANTS OF THE SUBTHRESHOLD VOLTAGE PDF

In this appendix, we compute the cumulants of the neuronal voltage $v_j(t)$ given by Eq. (13), which were used in the argument presented in Sec. IV B 1.

We revisit the neuronal voltage $v_j(t)$ in Eq. (13), which was derived from the differential equation (1) for the time period between total firing events. Since the external drive to any neuron is given by a Poisson spike train, at any given time $t > 0$, the number $M(t)$ of the spike times s_{ji} that have arrived at the neuron by this time is Poisson distributed with mean νt , and their locations can be considered as generated independently from the uniform distribution over the time interval $0 < s < t$ [78]. Therefore, for statistical purposes, we can rewrite Eq. (13) as

$$v(t) = V_R + \sum_{l=1}^{M(t)} f e^{-g_L[t - U_l(t)]}, \quad (\text{B1})$$

where the random variables $U_l(t)$, $l=1, \dots, M(t)$, are independent and uniformly distributed between 0 and t . Equivalently, $v(t)$ is the sum of a random number, $M(t)$, of independent random variables, each identically distributed over the r -interval $f e^{-g_L t} \leq r \leq f$ with the pdf $1/r g_L t$.

We next find the cumulants of $v(t)$ in Eq. (B1) by repeated differentiation of the cumulant generating function, $\Phi_v(k) = \ln \langle e^{ikv(t)} \rangle$ [78]. For the sum in Eq. (B1) of a random number of independent and identically distributed random variables, the characteristic function $\langle e^{ikv(t)} \rangle$ is the composition of the probability generating function $\langle s^{M(t)} \rangle = \exp(\nu t(s-1))$ of the Poisson-distributed number of spikes and the characteristic function of each term in the sum [78], and equals

$$\Phi_v(k) = ikV_R + \nu t \left[\frac{1}{g_L t} \int_{fe^{-g_L t}}^f \frac{e^{ikr}}{r} dr - 1 \right]. \quad (\text{B2})$$

The n th cumulant $c_n[v(t)]$ of the voltage in Eq. (B1) is given by the expression

$$c_n[v(t)] = (-i)^n \frac{d^n \Phi_v(k)}{dk^n} \Big|_{k=0},$$

which gives the mean voltage $c_1[v(t)]$ as in Eq. (14b), and

$$c_n[v(t)] = \frac{f^n \nu}{ng_L} (1 - e^{-ng_L t}) \quad (\text{B3})$$

for $n \geq 2$. In particular, the voltage variance is given by Eq. (14c).

We find, in particular, that the n th cumulant of the voltage is of order $O(\nu f^n)$. [The $O(f^n)$ dependence of the cumulants follows simply from the appearance of the spike strength, f , as a multiplicative constant in the random terms of the sum in Eq. (13)]. In the small-fluctuation regime, we demand that $f\nu = O(1)$ while taking $f \ll g_L(V_T - V_R)$ and $\nu \gg g_L$, and so we find that the mean voltage is $O(1)$ and its standard deviation is $O(\sqrt{\nu f})$. Therefore, the n th order cumulants of the pdf of

the voltage in Eq. (13), normalized with respect to its standard deviation, will scale as $(\nu f^n)/(\sqrt{\nu f})^n \sim O(\nu^{1-n/2})$, which is indeed negligible for $n \geq 3$.

APPENDIX C: ASYMPTOTIC FOR APPROXIMATION OF AVERAGE MAXIMAL VOLTAGE

Here, we derive the approximate formula (24) for the maximal value $y_{\max}(N)$ of the pdf $g^{(N)}(y)$ in Eq. (19). From the definition of the function $\text{erf}(\cdot)$ in Eq. (15), we find that $y_{\max}(N)$ solves the equation $\sqrt{\pi}y/\sqrt{2}[1 + \text{erf}(y/\sqrt{2})] = (N-1)e^{-y^2/2}$. For $y \geq 0$, the left-hand side of this equation is an increasing function of y , beginning with zero value at $y=0$, while the right-hand side is a decaying function of y . Therefore, this equation has a unique solution. As the left-hand side is clearly smaller than the right-hand side for $y=O(1)$ and $N \gg 1$, we know that the solution must satisfy $y \gg 1$. Using the large- z asymptotic expansion $\text{erf}(z) \sim 1 - e^{-z^2}/\sqrt{\pi}z + O(e^{-z^2}/z^3)$, we consequently derive the approximate equation $\sqrt{2}\pi y = Ne^{-y^2/2} + O(Ne^{-y^2/2}/y^2)$, valid for large N and y . At the leading order, this equation can be rewritten as $y^2 = \ln(N^2/2\pi) - \ln y^2$, and two iterations produce the approximation in Eq. (24).

-
- [1] R. Traub, J. Jeffreys, and M. Whittington, *Fast Oscillations in Cortical Circuits* (MIT Press, Cambridge, MA, 1999).
- [2] G. Buzsaki and A. Draguhn, *Science* **304**, 1926 (2004).
- [3] T. J. Sejnowski and O. Paulsen, *J. Neurosci.* **26**, 1673 (2006).
- [4] M. Steriade, *Neuroscience* **137**, 1087 (2006).
- [5] A. K. Roopun, M. A. Kramer, L. M. Carracedo, M. Kaiser, C. H. Davies, R. D. Traub, N. J. Kopell, and M. A. Whittington, *Front Neurosci.* **2**, 145 (2008).
- [6] P. Fries, *Annu. Rev. Neurosci.* **32**, 209 (2009).
- [7] W. Singer, *Neuron* **24**, 49 (1999).
- [8] E. H. Buhl, G. Tamas, and A. Fisahn, *J. Physiol.* **513**, 117 (1998).
- [9] A. Fisahn, F. G. Pike, E. H. Buhl, and O. Paulsen, *Nature (London)* **394**, 186 (1998).
- [10] J. M. Fellous and T. J. Sejnowski, *Hippocampus* **10**, 187 (2000).
- [11] N. K. Logothetis, J. Pauls, M. Augath, T. Trinath, and A. Oeltermann, *Nature (London)* **412**, 150 (2001).
- [12] P. Fries, J. H. Reynolds, A. E. Rorie, and R. Desimone, *Science* **291**, 1560 (2001).
- [13] N. Brunel and X.-J. Wang, *J. Neurophysiol.* **90**, 415 (2003).
- [14] G. Buzsaki, Z. Horvath, R. Urioste, J. Hetke, and K. Wise, *Science* **256**, 1025 (1992).
- [15] A. Bragin, G. Jando, Z. Nadasdy, J. Hetke, K. Wise, and G. Buzsaki, *J. Neurosci.* **15**, 47 (1995).
- [16] J. Csicsvari, H. Hirase, A. Czurko, and G. Buzsaki, *Neuron* **21**, 179 (1998).
- [17] J. Csicsvari, H. Hirase, A. Czurko, A. Mamiya, and G. Buzsaki, *J. Neurosci.* **19**, 274 (1999).
- [18] J. A. Henrie and R. Shapley, *J. Neurophysiol.* **94**, 479 (2005).
- [19] M. B. Feller, *Neuron* **22**, 653 (1999).
- [20] M. J. O'Donovan, *Curr. Opin. Neurobiol.* **9**, 94 (1999).
- [21] C. van Vreeswijk and D. Hansel, *Neural Comput.* **13**, 959 (2001).
- [22] B. B. Vladimirovski, J. Tabak, M. J. O'Donovan, and J. Rinzel, *J. Comput. Neurosci.* **25**, 39 (2008).
- [23] W. H. Nesse, A. Borisyuk, and P. C. Bressloff, *J. Comput. Neurosci.* **25**, 317 (2008).
- [24] R. E. Mirollo and S. H. Strogatz, *SIAM J. Appl. Math.* **50**, 1645 (1990).
- [25] N. Brunel and V. Hakim, *Neural Comput.* **11**, 1621 (1999).
- [26] C. Borgers and N. Kopell, *Neural Comput.* **15**, 509 (2003).
- [27] C. Borgers and N. Kopell, *Neural Comput.* **17**, 557 (2005).
- [28] D. Hansel, G. Mato, and C. Meunier, *Neural Comput.* **7**, 307 (1995).
- [29] W. W. Lytton and T. J. Sejnowski, *J. Neurophysiol.* **66**, 1059 (1991).
- [30] C. Van Vreeswijk L. F. Abbott, and G. B. Ermentrout, *J. Comput. Neurosci.* **1**, 313 (1994).
- [31] X.-J. Wang and G. Buzsaki, *J. Neurosci.* **16**, 6402 (1996).
- [32] C. C. Chow, J. A. White, J. Ritt, and N. Kopell, *J. Comput. Neurosci.* **5**, 407 (1998).
- [33] P. H. Tiesinga and J. V. Jose, *Network* **11**, 1 (2000).
- [34] M. A. Whittington, R. D. Traub, N. Kopell, G. B. Ermentrout, and E. H. Buhl, *Int. J. Psychophysiol.* **38**, 315 (2000).
- [35] R. Maex and E. D. Schutter, *J. Neurosci.* **23**, 10503 (2003).
- [36] N. Brunel, *J. Comput. Neurosci.* **8**, 183 (2000).
- [37] P. H. E. Tiesinga, J.-M. Fellous, J. V. José, and T. J. Sejnowski, *Hippocampus* **11**, 251 (2001).
- [38] D. Hansel and G. Mato, *Neural Comput.* **15**, 1 (2003).
- [39] R. D. Traub, A. Bibbig, A. Fisahn, F. E. N. LeBeau, M. A. Whittington, and E. H. Buhl, *Eur. J. Neurosci.* **12**, 4093 (2000).
- [40] R. D. Traub, M. O. Cunningham, T. Gloveli, F. E. N. LeBeau,

- A. Bibbig, E. H. Buhl, and M. A. Whittington, *Proc. Natl. Acad. Sci. U.S.A.* **100**, 11047 (2003).
- [41] R. D. Traub, I. Pais, A. Bibbig, F. E. N. LeBeau, E. H. Buhl, S. G. Hormuzdi, H. Monyer, and M. A. Whittington, *Proc. Natl. Acad. Sci. U.S.A.* **100**, 1370 (2003).
- [42] W. Gerstner, J. L. van Hemmen, and J. D. Cowan, *Neural Comput.* **8**, 1653 (1996).
- [43] C. C. Chow, *Physica D* **118**, 343 (1998).
- [44] J. A. White, C. C. Chow, J. Rit, C. Soto-Trevino, and N. Kopell, *J. Comput. Neurosci.* **5**, 5 (1998).
- [45] H. C. Tuckwell, *Introduction to Theoretical Neurobiology: Volume 2, Nonlinear and Stochastic Theories*, Cambridge Studies in Mathematical Biology (Cambridge University Press, Cambridge, England, 1988).
- [46] A. N. Burkitt, *Biol. Cybern.* **95**, 1 (2006).
- [47] A. N. Burkitt, *Biol. Cybern.* **95**, 97 (2006).
- [48] Y. Kuramoto, *Physica D* **50**, 15 (1991).
- [49] W. Senn and R. Urbanczik, *SIAM J. Appl. Math.* **61**, 1143 (2000).
- [50] N. Brunel and S. Sergi, *J. Theor. Biol.* **195**, 87 (1998).
- [51] R. M. Capocelli and L. M. Ricciardi, *Biol. Cybern.* **8**, 214 (1971).
- [52] P. Diťa, *J. Phys. A* **18**, 2685 (1985).
- [53] S. Sato, *Math. Biosci.* **39**, 53 (1978).
- [54] T. Shimokawa, K. Pakdaman, T. Takahata, S. Tanabe, and S. Sata, *Biol. Cybern.* **83**, 327 (2000).
- [55] V. Lánská, P. Lánský, and C. Smith, *J. Theor. Biol.* **166**, 393 (1994).
- [56] R. Brette, M. Rudolph, T. Carnevale, M. Hines, D. Beeman, J. M. Bower, M. Diesmann, A. Morrison, P. H. Goodman, F. C. Harris, Jr. *et al.*, *J. Comput. Neurosci.* **23**, 349 (2007).
- [57] D. P. Bertsekas and J. N. Tsitsiklis, *Introduction to Probability*, 2nd ed. (Athena Scientific, Nashua, NH, 2008), Sec. 4.1,
- [58] K. A. Newhall, G. Kovačič, P. R. Kramer, D. Zhou, A. V. Rangan, and D. Cai, *Commun. Math. Sci.* **8**, 541 (2010).
- [59] S. Sato, *J. Appl. Probab.* **14**, 850 (1977).
- [60] D. Cai, L. Tao, A. V. Rangan, and D. W. McLaughlin, *Commun. Math. Sci.* **4**, 97 (2006).
- [61] A. V. Rangan, G. Kovačič, and D. Cai, *Phys. Rev. E* **77**, 041915 (2008).
- [62] L. E. Reichl, *A Modern Course in Statistical Physics*, 2nd ed. (Wiley-Interscience, 1998).
- [63] D. Nykamp and D. Tranchina, *J. Comput. Neurosci.* **8**, 19 (2000).
- [64] C. W. Gardiner, *Handbook of Stochastic Methods*, 3rd ed. (Springer, 2004).
- [65] J. Thomas, *Numerical Partial Differential Equations: Finite Difference Methods* (Springer, New York, 1998).
- [66] R. E. L. DeVille and C. S. Peskin, *Bull. Math. Biol.* **70**, 1608 (2008).
- [67] P. L. Nunez, *Neocortical Dynamics and Human EEG Rhythms* (Oxford University Press, New York, Oxford, 1995).
- [68] V. Bringuier, F. Chavane, L. Glaeser, and Y. Fregnac, *Science* **283**, 695 (1999).
- [69] R. Eckhorn, A. M. Gail, A. Bruns, A. Gabriel, B. Al-Shaikhli, and M. Saam, *IEEE Trans. Neural Netw.* **15**, 1039 (2004).
- [70] M. Shelley and L. Tao, *J. Comput. Neurosci.* **11**, 111 (2001).
- [71] G. Kovačič, L. Tao, A. V. Rangan, and D. Cai, *Phys. Rev. E* **80**, 021904 (2009).
- [72] D. Zhou, Y. Sun, A. V. Rangan, and D. Cai, *J. Comput. Neurosci.* **28**, 229 (2010).
- [73] Y. Sun, D. Zhou, A. V. Rangan, and D. Cai, *J. Comput. Neurosci.* **28**, 247 (2010).
- [74] D. Zhou, A. V. Rangan, Y. Sun, and D. Cai, *Phys. Rev. E* **80**, 031918 (2009).
- [75] K. A. Newhall, M. Shkarayev, P. Kramer, G. Kovačič, and D. Cai, *Phys. Rev. E* (to be published).
- [76] *Handbook of Mathematical Functions*, 9th ed., edited by M. Abramowitz and I. A. Stegun (Dover Publications, Inc., New York, 1972).
- [77] L. J. Slater, *Confluent Hypergeometric Functions* (Cambridge University Press, New York, 1960).
- [78] S. Karlin and H. M. Taylor, *A First Course in Stochastic Processes*, 2nd ed. (Academic, Boston, 1975).